CHINESE JOURNAL OF MECHANICAL ENGINEERING
Vol. 27, No. 2, 2014

DOI: 10.3901/CJME.2014.02.428, available online at www.springerlink.com; www.cjmenet.com; www.cjmenet.com.cn

Excitation and Detection of Shear Horizontal Waves with Electromagnetic Acoustic Transducers for Nondestructive Testing of Plates

MA Qingzeng[1], JIAO Jingpin[2, *], HU Ping[1], ZHONG Xi[2], WU Bin[2], and HE Cunfu[2]

1 *Electric Power Research Institute of Guangdong Power Grid Corporation, Guangzhou 510600, China*
2 *College of Mechanical Engineering and Applied Electronics Technology, Beijing University of Technology, Beijing 100124, China*

Received May 29, 2013; revised October 11, 2013; accepted November 8, 2013

Abstract: The fundamental shear horizontal(SH0) wave has several unique features that are attractive for long-range nondestructive testing(NDT). By a careful design of the geometric configuration, electromagnetic acoustic transducers(EMATs) have the capability to generate a wide range of guided wave modes, such as Lamb waves and shear-horizontal(SH) waves in plates. However, the performance of EMATs is influenced by their parameters. To evaluate the performance of periodic permanent magnet(PPM) EMATs, a distributed-line-source model is developed to calculate the angular acoustic field cross-section in the far-field. Numerical analysis is conducted to investigate the performance of such EMATs with different geometric parameters, such as period and number of magnet arrays, and inner and outer coil widths. Such parameters have a great influence on the directivity of the generated SH0 waves that arises mainly in the amplitude and width of both main and side lobes. According to the numerical analysis, these parameters are optimized to obtain better directivity. Optimized PPM EMATs are designed and used for NDT of strip plates. Experimental results show that the lateral boundary of the strip plate has no perceivable influence on SH0-wave propagation, thus validating their used in NDT. The proposed model predicts the radiation pattern of PPM EMATs, and can be used for their parameter optimization.

Keywords: electromagnetic acoustic transducers, shear-horizontal waves, strip plate, nondestructive testing

1 Introduction

Guided wave inspection has proven to be a very effective method for the rapid inspection of large structures. In such inspections, accurate and efficient nondestructive evaluations are significantly affected by the characteristics of the guided waves, such as dispersion, wave structure, excitability, and directivity[1–3]. Compared with Lamb waves, the fundamental shear-horizontal(SH0) wave has several unique features that are attractive for long-range nondestructive testing(NDT). First, it is completely non-dispersive, which makes the interpretation of signals easier. Second, the out-of-plane particle displacement of the SH0 mode is zero, thus it is not affected by the presence of surrounding media. Moreover, the displacement of the SH0 wave is uniform through the whole thickness of the plate, thus its sensitivity to defects is independent of the through-thickness location of defects[4–6].

Guided waves can be generated by either piezoelectric transducers or electromagnetic acoustic transducers (EMATs). EMATs have recently attracted significant attention owing to their advantages over traditional piezoelectric transducers[7]. The contactless feature of EMATs overcomes the need for a couplant. Another attractive feature is their capability to generate a wide range of guided wave modes such as Lamb waves, surface wave, and shear-horizontal(SH) waves in plate-like structures by careful design of the geometric configuration of EMATs[8–10].

Generally, there are two kinds of transduction mechanisms: the Lorentz force and magnetostriction, which enable EMATs to generate and detect ultrasonic waves. In some cases these two mechanisms are additive, such as in the generation of bulk shear waves[11]. However, the configurations for generation of SH waves are different depending on the transduction phenomena. This results in two main classes of transducers(as shown in Fig. 1): periodic permanent magnet(PPM) EMATs, which are based on the Lorentz force[12–13], and planar solenoid array(PSA) EMATs, which are based on magnetostrictive effects occurring in the sample itself or in a strip of highly magnetostrictive material bonded to the sample[14–15]. Both schemes are employed in practical applications, but they have distinct features.

* Corresponding author. E-mail: jiaojp@bjut.edu.cn
This project is supported by National Natural Science Foundation of China(Grant Nos. 51075012, 10772008), and Beijing Municipal Natural Science Foundation of China(Grant No. 1122005)

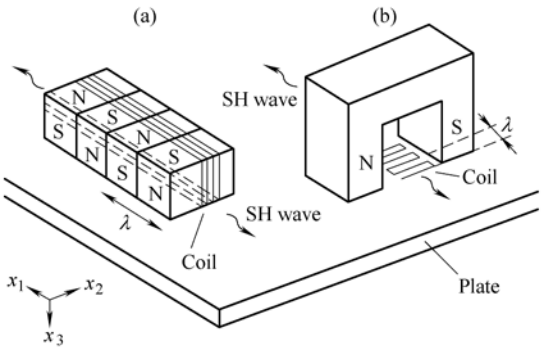

Fig. 1 Illustrations of (a) PPM and (b) PSA EMATs for exciting SH0 waves

The Lorentz force mechanism is linear and less sensitive to electromagnetic properties. In contrast, magnetostriction is highly nonlinear and its performance in SH-wave generation and reception depends significantly on the magnetic bias field and the physical properties of the sample[16]. Previous research claimed that the magnitude of the magnetostriction force can be as much as two orders larger than that of the Lorentz force in ferritic steels[17]. Recently, RIBICHINI, et al[18], demonstrated that the role of magnetostriction was overestimated because of an incorrect assumption of the mechanical boundary conditions. The magnitude of the magnetostriction force is typically found not to be an order larger than the Lorentz force; indeed, the Lorentz force is actually larger than magnetostriction force in non-oxidized ferromagnetic steels.

The electro-acoustic converting efficiency of EMAT is highly dependent on its structural parameters and material properties[19]. To improve the sensitivity of an EMAT, researchers investigated the influence of structural parameters and material properties on performance. RIBICHINI, et al[11], assessed their material-dependent behavior when used in inspecting different types of steel. The Lorentz force is shown to be the dominant transduction effect, and it is not significantly sensitive to the typical range of physical properties of steels. Therefore, the EMAT can be used on different grades of ferritic steel. HUANG, et al[20], investigated the effect of a static bias magnetic field on EMAT sensitivity. Numerical analysis was conducted to calculate the distribution of magnetic induction intensity and eddy current density produced by permanent magnet with different structural parameters. The results show that sensitivity is affected by the thickness of permanent magnet and the distance to the coil. According to these dependences, the design of the transducer was optimized. WILCOX, et al[21], investigated the excitation and detection of Lamb waves in nonferromagnetic metallic waveguides using planar EMATs. A model was developed to calculate the radiate acoustic field of the planar coil EMAT. It was used to analyze the different effects that contribute to the overall Lamb wave modal sensitivity of the EMAT. Both inner and outer coil diameters determine the wavelengths at which minima in sensitivity occur. Thus, it is relatively straightforward to design an EMAT coil to suppress an undesired guided wave mode of a particular wavelength. RIBICHINI, et al[22], compared the performance of PPM EMAT and magnetostriction EMAT in exciting SH waves on steel structures. Finite element analysis was performed to quantitatively assess the dependence of wave amplitude on key design parameters. The magnetostrictive EMATs directly applied on mild steel plates showed relatively poor performance owing to a strong dependence on the magneto-mechanical properties of the test sample. PPM EMATs generate ultrasonic waves of intermediate amplitude and are insensitive to variations in material properties. Meanwhile, it is found that a layer of highly magnetostrictive material attached between the transducer and the plate can help to enhance ultrasonic-wave amplitudes.

Concerning the influence of directivity on the performance of NDT, LEE, et al[23], developed a general model to investigate the influence of the solenoid interval in PSA EMATs on the directivity of the generated SH0 wave. The radiation patterns obtained from the experiments agrees well with the numerical results.

Our investigation was concerned with the improvement of the performance of PPM EMATs for SH0 wave excitation and reception. In section 1, a general model is described that predicts the operation of PPM EMATs as transmitters and receivers of SH0 waves. In section 2, numerical results of the parameters of PPM EMATs that affect the performance of generated SH0 waves are presented. In section 3, optimized values of the parameters of PPM EMATs according to the numerical analysis are given, and excitation and reception of SH0 waves in plates using fabricated EMATs are described.

2 Theoretical Model of PPM EMATs

To investigate the influence of the geometric configuration of a meander-line coil and magnet on performance of EMATs, a theoretical analysis was performed. The line-source model employed in Ref. [23] was modified for the present problem.

The proposed PPM EMATs consist of a planar solenoid and N pairs of magnets (Fig. 2(a)). The central distance of each pair of magnets is denoted as l_p. It is assumed that the magnetic field mainly exists in the rectangular region covered by the magnets. Consequently, the excitation shearing deformations are mainly limited in the strip regions (Fig. 2(b)), and the central distances of the strips are the coil span ζ.

If the receiver is located in the far-field of the transmitter, the shearing deformations in the strips can be considered as distributed line sources. The far-field response of the PPM EMATs is the superposition of the acoustic fields generated by the line sources in ranges (from $-D/2$ to $-d/2$) and

(from $d/2$ to $D/2$), as shown in Fig. 2(b), where D is the outer width of the meander-line coil, and d is its inner width. This coil is uniform, and ξ is the spacing in the coil, which is equal to the central distance between strips. Therefore, the number of line sources M is determined by widths D and d. The length of the line sources L is equal to the width of the magnet array $L = ND_p$, where D_p is the width of each magnet. The far-field response R_m induced by a single line source m is calculated first as follows.

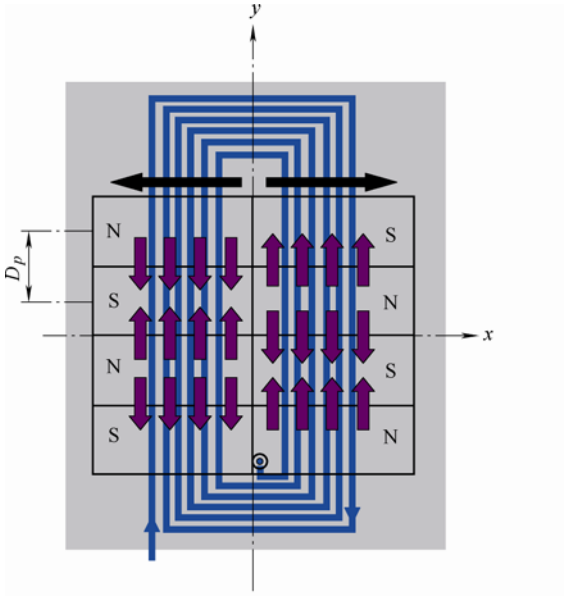

(a) Distribution of the magnetic field induced by PPM EMAT

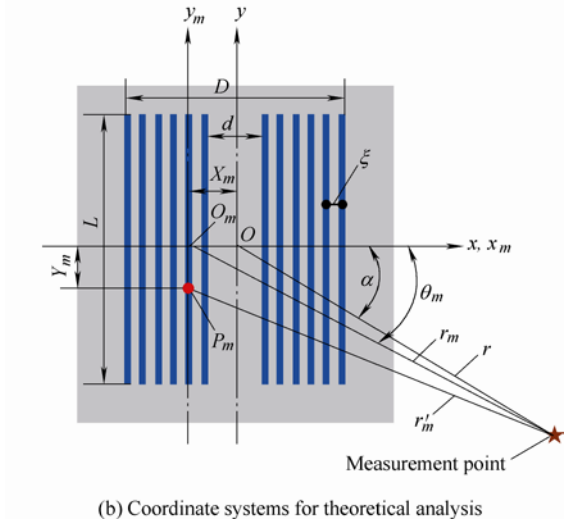

(b) Coordinate systems for theoretical analysis

Fig. 2 Model for acoustic field analysis of PPM EMATs

Based on Huygens' principle, the far-field response(R_m) of the line source can be calculated by integrating the far-field response(R_p) of a point source located at P_m over the length L, as indicated in Fig. 2(b). The length of each point source should be less than a quarter of the shortest wavelength of the SH wave considered. The far-field response of a harmonic point source located at P_m ($x = X_m$, $y = Y_m$) can be described as follows[24]:

$$R_p \approx \sqrt{\frac{2}{\pi k r'_m}} \exp\left(\mathrm{j}\left(k r'_m - \omega t + \frac{\pi}{4}\right)\right), \tag{1}$$

where r'_m is the distance from P_m to the measurement point. For convenience, a local coordinate system whose origin is located at the center (O_m, (x_m, y_m)) of the strip m is introduced. In Eq. (1), ω is the angular frequency and k is the wavenumber.

If the source strength at P_m is $A_m \mathrm{d}y_m$, and A_m is a constant, the far-field response R_m of line source can be obtained by integrating R_p over L_m:

$$R_m(r_m, \theta_m, t) = \int_{-\frac{L}{2}}^{\frac{L}{2}} A_m R_p \,\mathrm{d}y_m =$$

$$A_m \int_{-\frac{L}{2}}^{\frac{L}{2}} \sqrt{\frac{2}{\pi k r'_m}} \exp\left(\mathrm{j}\left(k r'_m - \omega t + \frac{\pi}{4}\right)\right) \mathrm{d}y_m . \tag{2}$$

As the measurement is conducted at the far-field (r'_m ? L), it can be assumed that

$$r'_m = r_m - y_m \sin\theta_m . \tag{3}$$

Substituting Eq. (3) into Eq. (2) gives

$$R_m(r_m, \theta_m, t) \approx A_m \int_{-\frac{L}{2}}^{\frac{L}{2}} \sqrt{\frac{2}{\pi k (r_m - y_m \sin\theta_m)}} \times$$

$$\exp\left(\mathrm{j}\left(k r_m - k y_m \sin\theta_m - \omega t + \frac{\pi}{4}\right)\right) \mathrm{d}y_m \approx$$

$$A_m \sqrt{\frac{2}{\pi k r_m}} \exp\left(\mathrm{j}\left(k r_m - \omega t + \frac{\pi}{4}\right)\right) \int_{-\frac{L}{2}}^{\frac{L}{2}} \exp\left(-\mathrm{j}(k y_m \sin\theta_m)\right) \mathrm{d}y_m \approx$$

$$A_m L \sqrt{\frac{2}{\pi k r_m}} \exp\left(\mathrm{j}\left(k r_m - \omega t + \frac{\pi}{4}\right)\right) \left[\frac{\sin\left(\frac{1}{2} k L \sin\theta_m\right)}{\frac{1}{2} k L \sin\theta_m}\right]. \tag{4}$$

By summing R_m for $m = 1, 2, \cdots, M$, the total response at a measurement point (x,y) or (r,a) induced by all distributed line sources can be obtained:

$$R(r, \alpha, t) = \sum_{m=1}^{M} A_m L \sqrt{\frac{2}{\pi k r_m}} \exp\left(\mathrm{j}\left(k r_m - \omega t + \frac{\pi}{4}\right)\right) \left[\frac{\sin\left(\frac{1}{2} k L \sin\theta_m\right)}{\frac{1}{2} k L \sin\theta_m}\right], \tag{5}$$

where

$$r_m = \sqrt{(r\sin\alpha)^2 + (r\cos\alpha - X_m)^2}\,, \tag{6a}$$

$$\theta_m = \arctan\left(\frac{r\sin\alpha}{r\cos\alpha - X_m}\right). \tag{6b}$$

In Eq. (6), X_m is the distance between the origin of global coordinate system(O) and the origin of the local coordinate system(O_m). Because the source strength A_m depends on the applied magnetic field strength, it cannot be constant but is assumed to be uniform in each strip m. Note that the signs of the shearing stress in the adjacent strips are different, i.e., if the shear stress in the second strip is positive, then the shear stress in the first and third strips are negative. Thus the applied magnetic field strength can be simplified as

$$A_m = (-1)^m A_0 . \tag{7}$$

Therefore, $R(r,\alpha,t)$ can be rewritten as

$$R(r,\alpha,t) = A_0\sqrt{\frac{2}{\pi k}}\exp\left(-\mathrm{j}\left(\omega t-\frac{\pi}{4}\right)\right)\times \sum_{m=1}^{M}(-1)^m\left\{\frac{L}{\sqrt{r_m}}\left[\frac{\sin\left(\frac{1}{2}kL\sin\theta_m\right)}{\frac{1}{2}kL\sin\theta_m}\right]\right\}\exp\left(\mathrm{j}kr_m\right). \tag{8}$$

This is the fundamental equation that is used for modeling the performance of PPM EMATs in our study. It is also valid for devices that can be regarded as distributed line sources.

3 Numerical analysis of Radiate Acoustic Field of different EMATs

Physically, Eq. (8) represents the superimposition of the far-field responses from multiple line sources, which is a function of the number of line sources M and the length of line sources $L = ND_p$. In this section, the model is used to investigate how these parameters affect the operation of PPM EMATs, and to determine some basic principles for transducer design.

3.1 Effect of period of magnet array

For PPM EMATs, the mode selection and frequency tuning are determined by the period of the permanent magnets D_p, which is equal to half the wavelength of the excited waves. The relationship between the period of the magnet and the central frequency (or the wavelength) of the SH0 wave is listed in Table 1 for a 5.9-mm-thick steel plate. The table shows that the central frequency of transducer increases with the decrease of periods of the magnet array.

Table 1. Parameters of EMATs for SH0 wave excitation

Number	Period D_p/mm	Wavelength λ/mm	Frequency f/kHz
1	13.0	26.1	125
2	6.3	12.5	260
3	5.3	10.5	310
4	3.3	6.5	500

Based on the above model, calculations were performed to investigate the effect of the inner width of the coil on the radiation pattern of the waves. In these simulations, only the period of the magnet D_p was varied; all other parameters were fixed. The periods of the magnet array are 3.3 mm, 5.3 mm, 6.3 mm, and 13 mm. The magnet array contain four pairs of magnets, and the outer and inner widths of the coil were 20 mm and 6 mm. Fig. 3 shows the angular acoustic field cross-section at a distance of 400 mm generated by these EMATs.

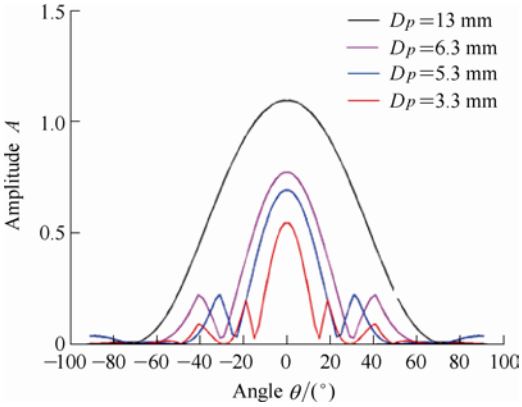

Fig. 3 Directivity of EMATs differ in period of magnet array

Clearly, the period of the magnet array has a large effect on the radiation pattern of the waves. As the period decreases, the width of the main lobe becomes narrower, indicating that the directivity of the generated wave is improved. However, the improvement is accompanied by a decrease in the amplitude of the main lobe, and an increase in the amplitude of the side lobes. Thus the PPM EMATs have a poorer capability for long distance inspection resulting from the decrease in the period of the magnet array. Therefore, in determining the period, the effect on the amplitude and width of the main and side lobes should be considered.

3.2 Effect of Outer Coil Width of PPM EMATs

Similar to the above analysis, calculations were performed to examine the influence of the outer width of the coil on the performance of PPM EMATs. The inner width is 2 mm. The magnet array contain four pairs of magnets, and the period of the magnet array was 6.3 mm. Fig. 4 shows the angular acoustic field cross-section at distance of 400 mm generated by EMATs with outer coil widths of 10 mm, 20 mm, 30 mm, and 40 mm. The directivity of the generated wave is strongly dependent on the dimension of the coil's outer width. With increasing outer coil width, the beam steering performance of the EMAT improves. This is supported by the increase in the amplitude and a decrease in the width of the main lobe, although accompanied by an increase in the amplitude of the side lobes. Therefore, in determining the outer coil width, we have to balance beam steering against side-lobe

amplitude and the size of the transducer.

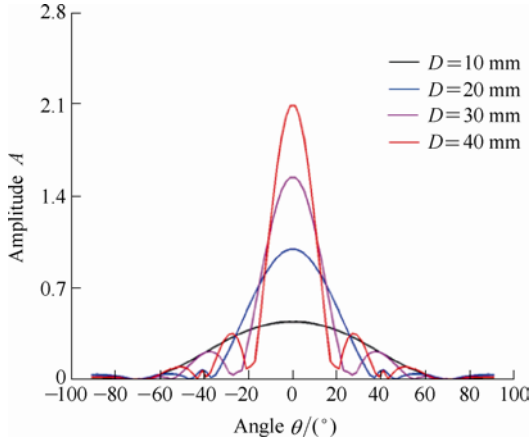

Fig. 4 Directivity of EMATs for different outer coil widths

3.3 Effect of Inner Coil Width of PPM EMATs

Similarly, calculations were performed to assess the influence of the outer width of the coil on performance. Fig. 5 shows the angular acoustic field cross-section at a distance of 400 mm for the EMATs with inner widths of 2 mm, 4 mm, 6 mm, and 8 mm. The outer width of the coil is 20 mm. The period and number of pairs of magnet arrays are the same as above ($N = 4$, $D_p = 6.3$ mm).

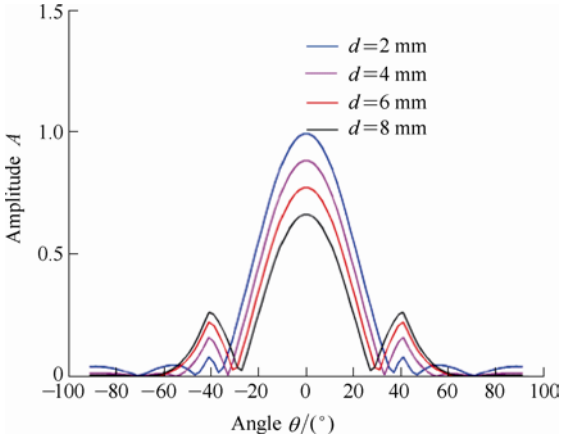

Fig. 5 Directivity of EMATs with different inner widths of coil

Clearly, decreasing the inner width of the coil increases the amplitude of the main lobe slightly and decreases the amplitude of the side lobe slightly; however, it is accompanied by a slight increase in the width of the main lobe. Therefore, in determining the inner width of the coil, the effect on the amplitude and the width of the main lobe should be considered.

3.4 Effect of number of magnet arrays

To evaluate the influence of the number of magnet arrays on the radiation pattern of waves, Fig. 6 shows the angular acoustic field cross-section at a distance of 400 mm for EMATs with different numbers of magnet arrays ($N = 3$, 4, 5, 6). The other parameters are the same for all PPM EMATs. The period of the magnet array is the same as above ($D_p = 6.3$ mm), the inner width of coil d is 2 mm, and the outer width D of the coil is 20 mm. The number of pairs of magnet arrays is found to have almost no effect on the directivity of transducers, although it does have an effect on the amplitude of the main lobe. Within the observed limits, the amplitude of the main lobe increases with increasing number of pairs of magnet arrays.

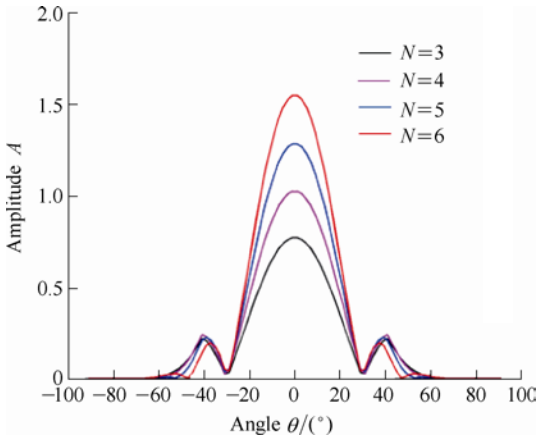

Fig. 6 Directivity of EMATs with different number of magnet arrays

In summary, the dimensions of the coil and magnet have a complex effect on the directivity of the generated SH0 waves from PPM EMATs. Therefore, according to the above numerical analysis, the parameters of the PPM EMATs should be optimized to obtain perfect acoustic field distributions.

4 Experimental Measurements

To improve the capability of PPM EMATs to excite and detect SH0 waves, EMAT parameters were optimized. Based on this optimization, PPM EMATs were designed, fabricated, and used in the NDT of plates.

4.1 Transducer design and experimental system

The group velocity dispersion curves of the SH waves in a 5.9 mm-thick infinite steel plate are shown in Fig. 7. The cutoff frequency of the SH1 wave is about 310 kHz. To keep the signal as simple as possible and avoid multimodality, the central frequency of the PPM EMATs is maintained above 310 kHz.

Considering the relationships between the period of the magnet and the central frequency of the SH0 wave (listed in Table 1), and the influence of the period of magnet on the directivity of the SH0 wave(see Fig. 2), the optimum

period of the magnet of the PPM EMATs should be greater than 5.3 mm. Based on the normal dimensions of the magnet provided by the manufacturer, the dimensions of the neodymium-iron-boron magnet were determined to be 20 mm × 8 mm × 6.5 mm, and the period of magnet array was D_p=6.5 mm. In each PPM EMATs, there are six pairs of magnets (Fig. 8).

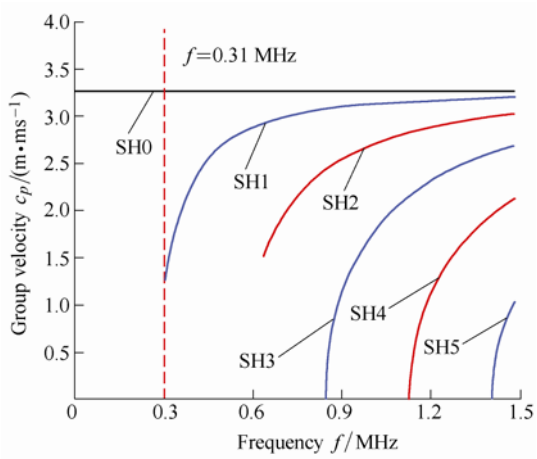

Fig. 7 Disperse curve of SH wave in 5.9 mm-thick steel plate

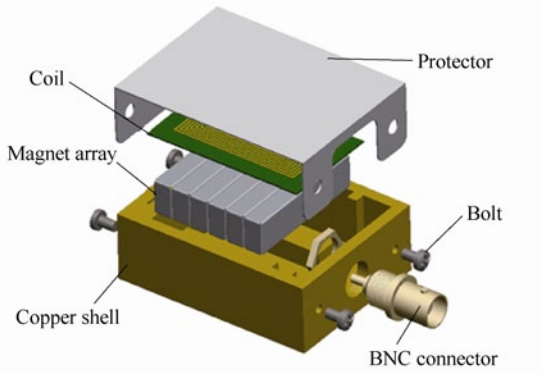

Fig. 8 Schematic of PPM EMATs

According to the numerical analysis, values for the dimensions of the coil were determined as follows: outer width D = 20 mm, inner width d = 2 mm, and length l = 30 mm. To ensure accurate control of the EMAT geometry, the coils were fabricated using printed circuit board(PCB) techniques. The dimensions of the PCB were 50 mm × 30 mm × 0.5 mm.

The fabricated EMATs were tested in a pitch-catch configuration, and a schematic of the instrumentation used is shown in Fig. 9. The transmitting EMAT is driven by a function generator, and amplified by a power amplifier, which is capable of transmitting tone bursts with peak voltages of about 150 V. The receiving EMAT was connected through a pre-amplifier to a channel of the digital storage oscilloscope. The oscilloscope is triggered by a timing signal delivered by a function generator that is synchronized with the transmitted waveform.

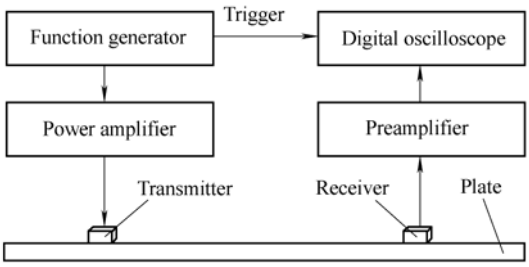

Fig. 9 Schematic of the experimental system

4.2 Measurement of beam directivity

To observe the radiation pattern of the PPM EMATs, experiments were performed on 5.9-mm-thick steel plates. The configuration of the PPM EMATs is shown in Fig. 10. The distance between transmitter and receiver is fixed at l_R = 400 mm, and the radiation angle θ is varied from −90° to 90° in increments of 15°. The experimental signals detected at different radiation angles are used in constructing the radiation patterns of the PPM EMATs.

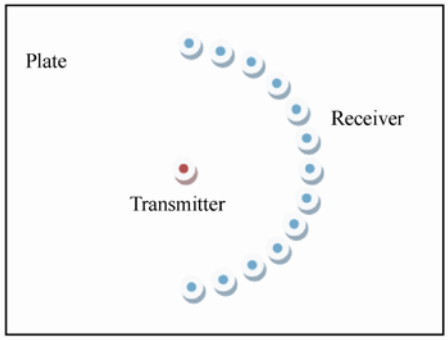

Fig. 10 Experimental configuration for directivity measurements

Fig. 11 shows the normalized peak-to-peak values of the signals measured at different radiation angles. The experimental data agrees well with the predicted radiation patterns. Thus, the distributed-line-source model developed in this investigation can be used in predicting these radiation patterns.

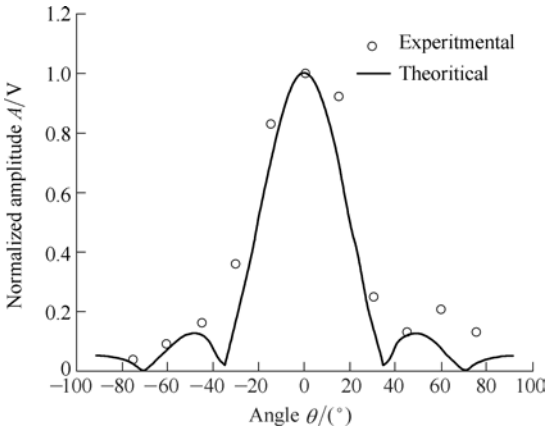

Fig. 11 Radiation patterns generated by PPM EMATs

4.3 Application in NDT of strip plates

To further establish perfect directivity of the fabricated PPM EMATs, these EMATs were used in NDT of a special plate with narrow width(strip plate), known as a grounding grid(see Fig. 12). Grounding grids are widely used in substations to guarantee the safe operation of power apparatus. The configuration for the strip plate experiments is shown in Fig. 13.

Fig. 12 Photo of strip plates for inspection

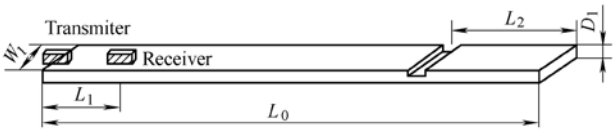

Fig. 13 Typical waveform of SH0 wave detected in strip plate

To demonstrate the potential of SH0 wave for NDT, three kinds of experiments were conducted: (1) experiments to show the propagation capability of SH0 waves in strip plates, (2) experiments to evaluate the sensitivity of SH0 waves to defects at different depth locations, and (3) experiments to investigate the influence of the surrounding environment on the propagation of SH0 waves. The values for the geometric parameters used in these experiments are listed in Table 2.

Table 2. Geometric parameters in experiments

Experiment No.	L_0/m	L_1/m	L_2/m	W_1/mm	D_t/mm
1	4	0.75		60	5.8
2	4	0.75	1	60	5.8
3	6	2	1	60	6.0

In experiment #1, there is no defect in the tested sample, and a typical waveform is shown in Fig. 14. In accordance with the group velocity of the SH0 wave, 3260 m/s, and the patial arrangement of transducers, the echoes in the detected signals are easy to determine. Besides the directive wave, the detected signal contains reflective echoes from the right and left ends of the strip plates, indicating that the lateral boundary has no perceptible influence on the propagation of SH0 waves in the strip plates because of its non-dispersion and no mode conversion at the lateral edges.

In experiment #2, contrastive tests were conducted to demonstrate the identical sensitivity of the SH0 wave to defects at different depth locations. A groove of 10 mm width and 2 mm depth was machined in the strip plate, at a distance 1 m away from the right end of the strip plate. In these contrastive tests, the transmitter was mounted on the top surface of the strip plate and the receiver was mounted at a fixed distance(L_1=0.75 m). However, the receiver was mounted at two different depth locations: one at the top surface of the plate, the other at the bottom surface.

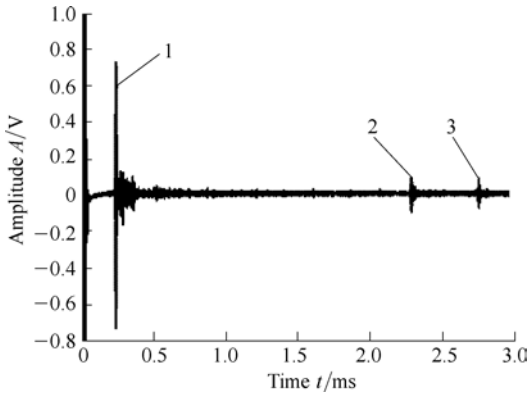

Fig. 14 Typical waveform of SH0 wave detected in strip plate

Fig. 15 shows typical results where the detected waveforms are almost identical with five recognizable echoes within 5 ms. The five echoes are the directive wave and reflective waves from the groove, groove-left end, right end, and right end-left ends. This demonstrates that the sensitivity of the SH0 wave to defects is independent of the through-thickness location of the defects.

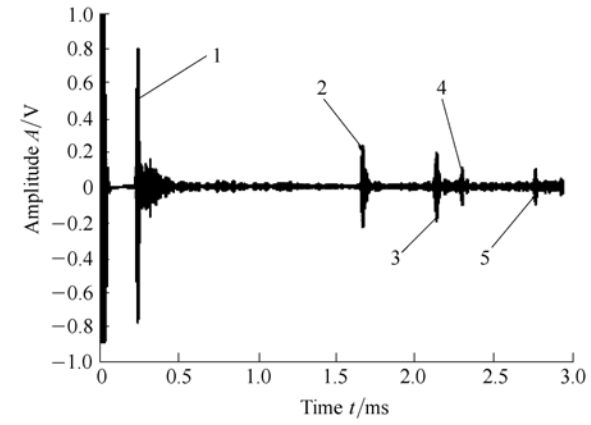

(a) On top surface

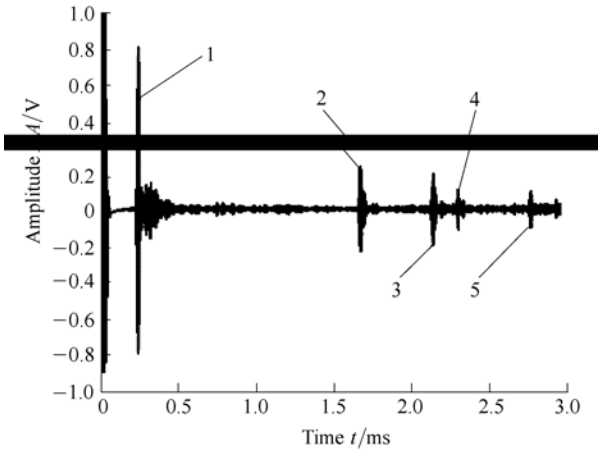

Fig. 15 Comparison of waveforms at different depths

To reveal the presence of surrounding media in the NDT of SH0 waves, contrastive tests were conducted on aother strip plate (as list in Table 2) when in air and buried in soil at 1-m depth. A smaller groove of 1-mm depth and 2-mm width was machined on the tested strip plate. The groove is 1 m away from the right end of the sample. The transmitter and the receiver were both mounted on the top surface of the sample, and their distance was L_1=2 m. Two typical waveforms are shown in Fig. 16.

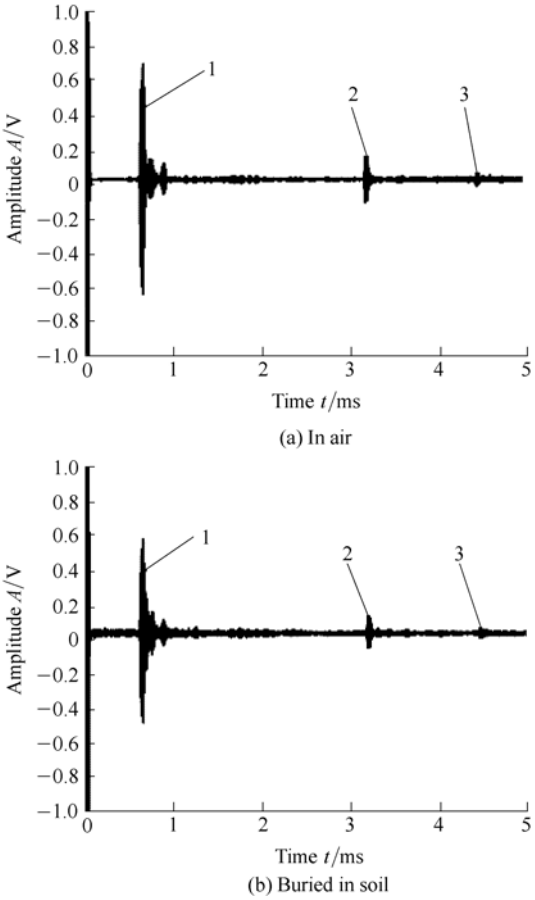

Fig. 16 Waveforms received in different environments

Both waveforms contain three echoes: the directive wave, the reflective wave from the defect, and the reflective wave from the right end. Therefore, in both cases the small groove can be detected, although for the buried case, there is obvious attenuation in the amplitude for all three echoes. Nevertheless, the SH0 wave is still an effective tool for NDT of a sample embedded in viscid media.

5 Conclusions

(1) A distributed-line-source model is developed for predicting the angular acoustic distribution in the far-field of PPM EMATs.

(2) Numerical analysis is conducted to investigate the performance of PPM EMATs of different geometries, such as period and number of magnet arrays, and inner and outer coil widths. The transducer parameters are shown to have a great influence on the directivity of generated SH0 wave, which affected amplitude and width of the main and side lobes.

(3) The PPM EMAT parameters are optimized to obtain better directivity by using numerical analysis of the acoustic field distribution,.

(4) Optimized PPM EMATs are fabricated and used in NDT of strip plates. Experimental results showe that the lateral boundary of the strip plate had no perceptible influence on the propagation of the SH0 wave arising from perfect directivity of transducers. Moreover, it is demonstrated that the SH0 wave has the potential to identify and measure embedded structures in NDT.

(5) The numerical and experimental results demonstrate that the distributed-line-source model is reliable in predicting radiation patterns of PPM EMATs, and can be used for the optimization of PPM EMATs.

References

[1] SU Z Q, YE L, LU Y. Guided Lamb waves for identification of damage in composite structures: A review[J]. *Journal of Sound and Vibration*, 2006, 295(1): 753–780.

[2] GAO H D, ROSE J L. Goodness dispersion curves for ultrasonic guided wave based SHM: a sample problem in corrosion monitoring [J]. *Aeronautical Journal*, 2010, 114(1 151): 49–56.

[3] LOWE M J S, DILIGENT O. Low-frequency reflection characteristics of the S0 Lamb wave from a rectangular notch in a plate[J]. *Journal of the Acoustical Society of America*, 2002, 111(1): 64–74.

[4] JIAO J P, ZHONG X, WU B, et al. Experiments on non-destructive testing of grounding grids using SH0 guided wave[J]. *Insight: Non-Destructive Testing and Condition Monitoring*, 2012, 54(7): 375–379.

[5] LIU Z H, WU B, HE C F, et al. Detection of longitudinal defect in pipes using torsional modes[J]. *Journal of Mechanical Engineering*, 2006, 19(1): 146–150.

[6] FAN Z, LOWE M J S. Torsional waves propagation along a waveguide of arbitrary cross section immersed in a perfect fluid[J]. *Journal of the Acoustical Society of America*, 2008, 124(4): 2002–2009.

[7] TSE P W, LIU X C, LIU Z H, et al. An innovative design for using flexible printed coils for magnetostrictive-based longitudinal guided wave sensors in steel strand inspection[J]. *Smart Materials and Structures*, 2011, 20(5): 1–6.

[8] WU, B, LI Y, ZHENG Y, et al. Thickness measurement of surface attachment on plate with SH wave[J]. *Journal of Mechanical Engineering*, 2012, 48(18): 77–83. (in Chinese)

[9] HUANG F Y, ZHOU Z G. Effect of static bias magnetic field on electromagnetic acoustic transducer sensitivity[J]. *Journal of Mechanical Engineering*, 2011, 47(10): 1–7.

[10] WANG, S J, KANG L, LI Z C. 3-D modeling and analysis of meander-line-coil surface wave EMATs[J]. *Mechatronics*, 2012, 22(6): 653–660.

[11] RIBICHINI R, CEGLA F, NAGY P B, et al. Experimental and numerical evaluation of electromagnetic acoustic transducer performance on steel materials[J]. *NDT & E International*, 2012, 45(1): 32–38.

[12] VASILE C F, THOMPSON R B. Excitation of horizontally polarized shear elastic waves by electromagnetic transducers with periodic permanent magnets[J]. *J. Appl. Phys.*, 1979, 50(4): 2583–2588.

[13] MAXFIELD B W, FORTUNKO C M. The design and use of electromagnetic acoustic wave transducers[J]. *Mater. Eval*., 1983, 41(12): 1399–1408.
[14] CHO S H, SUN K H, LEE J S, et al. Development of an orientation-adjustable path-type magnetostrictive sensor for damage detection in a plate[C]//*16th World Conference on Nondestructive Testing*, Montreal, Canada, September, 2004: 108–116.
[15] KWUN H, BARTELS K. Magnetostrictive sensor technology and its applications[J]. *Ultrasonics*, 1998, 36(1–5): 171–178.
[16] MURAYAMA R, MAKIYAMA S, KODAMA M, et al. Development of an ultrasonic inspection robot using an electromagnetic acoustic transducer for a Lamb wave and an SH-plate wave[J]. *Ultrasonics*, 2004, 42(1–9): 825–829.
[17] HIRAO M, OGI H. *EMATs for science and industry: noncontacting ultrasonic measurements*[M]. Boston: Kluwer Academic Publishers, 2003.
[18] RIBICHINI R, NAGY P B, OGI H. The impact of magnetostriction on the transduction of normal bias field EMATs[J]. *NDT & E International*, 2012, 51(1): 8–15.
[19] ROUGE C, LHEMERY A, SEGUR D. Modal solutions for SH guided waves radiated by an EMAT in a ferromagnetic plate[J]. *Journal of Physics: Conference Series*, 2012, 353(012014): 1–19.
[20] HUANG F Y, ZHOU Z G. Effect of static bias magnetic field on electromagnetic acoustic transducer sensitivity[J]. *Journal of Mechanical Engineering*, 2011, 47(10): 1–7. (in Chinese)
[21] WILCOX P D, LOWE M J S, CAWLEY P. The excitation and detection of Lamb waves with planar coil Electromagnetic Acoustic Transducers [J]. *IEEE Transactions on Ultrasonics, Ferroelectrics, and Frequency Control*, 2005, 52(12): 2370–2383
[22] RIBICHINI R, CEGLA F, NAGY P B, et al. Study and comparison of different EMAT configurations for SH wave inspection[J]. *IEEE Transactions on Ultrasonics, Ferroelectrics, and Frequency Control*, 2011, 58(12): 2571–2582.
[23] LEE J S, KIM Y Y, CHO S H. Beam-focused shear-horizontal wave generation in a plate by a circular magnetostrictive patch transducer employing a planar solenoid array[J]. *Smart Materials and Structures*, 2009, 18(1): 1–9.
[24] GRAFF K F. *Wave motion in elastic solid* [M]. New York: Oxford University Press, 1975.

Biographical notes

MA Qingzeng, born in 1971, is currently an engineer at *Electric Power Research Institute of Guangdong Power Grid Corporation*, *China*. He received his master's degree on thermal power engineering at *Wuhan University of Hydraulic and Electricity, China*, in 1996.
E-mail: mymdonald@163.com.

JIAO Jingpin, born in 1973, is currently a professor at *Beijing University of Technology, China*. He received his PhD degree in mechanical engineering in *Beijing University of Technology, China*, in 2005. Her research interests include transducers and measurements, and nondestructive testing techniques, such as guided wave, phased array, and nonlinear ultrasonic.
Tel: +86-10-67391720; E-mail: jiaojp@bjut.edu.cn.

HU Ping, born in 1973, is currently an engineer at *Electric Power Research Institute of Guangdong Power Grid Corporation, China*. She received her PhD degree in materials processing engineering in *South China University of Technology, China*, in 2001.
E-mail: horse2002hp@163.com.

ZHONG Xi, born in 1988, is currently a master's candidate at *Beijing University of Technology, China*.
E-mail: zhongxi@hotmail.com.

WU Bin, born in 1962, is currently a professor at *Beijing University of Technology*. He received his PhD degree from *Beihang University, China*, in 1997. His research interests include mechanical engineering, and ultrasonic nondestructive testing techniques.
E-mail: wb@bjut.edu.cn.

HE Cunfu, born in 1958, is currently a professor at *Beijing University of Technology*. He received his PhD degree from *Tsinghua University, China*, in 1996. His research interests include mechanical engineering, and ultrasonic nondestructive testing techniques.
E-mail: hecunfu@bjut.edu.cn.